# MONITORING LOCALIZED THIN-FILM CORROSION EVENTS VIA INTEGRATED OPTICAL AND ATOMIC FORCE MICROSCOPIES

Keith J. Stevenson[a], Joseph T. Hupp[a]
and Susan G. Yan[b]
(a) Department of Chemistry, Northwestern University,
2145 Sheridan Rd., Evanston, IL 60208
(b) Naval Undersea Warfare Center-Division Newport Code 8231,
Building 1302/2, Newport, RI 02841

Newly developed methodologies are presented in which localized corrosion of aluminum thin-films can be temporally and spatially imaged and subsequently correlated with structural characteristics. Preliminary experiments on microscopically patterned Al thin-films under open circuit conditions in two representative aqueous solutions (sea salt and hydrogen peroxide) are reported. Significant surface blistering (bubbles) due to excessive subsurface gas evolution occurs for Al films exposed to sea salt solutions, resulting in film delamination. In addition, pitting corrosion is observed, but at a slow rate. In contrast, the corrosion process for Al thin-films immersed in hydrogen peroxide solutions is dominated by pitting processes. Single micron-sized pits were observed to grow at a constant rate where the pit perimeter increased linearly with time. Initially, pit morphology was round and smooth, but at longer times the pits became less circular and rougher. Analysis of the data allowed for calculation of single pit current densities without resort to electrochemical extrapolation.

## INTRODUCTION

Of major practical interest is the development of new methods and techniques for the detection of localized corrosion and the study of corrosion processes. Recently, a variety of approaches have been reported for mapping localized corrosion activity, including high resolution scanning microscopies such as CLSM, SECM, PEM and NSOM (1-3). While these techniques provide high resolution surface maps, they are generally poorly suited for mass transfer investigations in that the imaging process is typically too slow (~1-30 min) and the probe itself often perturbs the diffusion profile of the electrochemical event. For this reason, several researchers have employed luminescence (4) and fluorescence (5) microscopies to characterize the spatial distribution of electrochemical activity on a surface. These methodologies are capable of following processes on faster time scales (generally milliseconds to seconds) by collecting light from a luminescence producing reaction or probe with an imaging detector (CCD). Additionally, chemical information (e.g., ion concentration and pH) can be obtained by choosing an appropriate spectroscopic (typically, chemiluminescent) probe molecule.

We also have become interested in the development of new methods to study localized corrosion processes. Of special concern, are parasitic corrosion reactions that occur at aluminum anodes employed in aluminum-based seawater semi-fuel cells (6). Direct reactions of both hydrogen peroxide fuel and supporting electrolyte (seawater) have been identified as factors limiting cell performance. In an effort to optimize battery performance and efficiency, we have chosen to obtain a more detailed evaluation of the chemical corrosion process (e.g., defect and impurity dependence, role of grain boundaries, role of oxide pitting, etc.). Due to the diversity of the chemistry and materials under study, we have chosen to take a "broad-based" approach by utilizing a single integrated instrument consisting of a free-standing atomic force microscope (AFM) mounted on the stage of an inverted optical microscope. This allows for greater experimental flexibility in that on-axis atomic force and optical images can be acquired subsequently (or simultaneously) on a sample of interest. By coupling high resolution surface maps with optical imaging techniques, localized corrosion activity can be examined on much faster time scales than conventional scanning probe microscopies. In this work, we describe newly developed methododologies for in-situ monitoring of localized corrosion of aluminum thin-films. Preliminary results from two "model" corrosion systems (Al/sea salt and Al/$H_2O_2$) are presented and used to illustrate the resolving power of this integrated approach.

## EXPERIMENTAL

Figure 1 illustrates the setup and instrumental configuration for integration of the optical and atomic force microscopies. All AFM measurements were obtained in contact mode. Fluorescence microscopy studies were performed by using the inverted microscope in an epi-fluorescence configuration. A 100 W mercury lamp was used together with a Nikon Plan Fluor (60 X /NA = 0.70) objective, a 365 nm band pass excitation filter, a 400 nm dichroic mirror and a 450 $\pm$ 65 nm band pass emission filter. Digital images were acquired with an intensified, precooled (-25 °C) CCD camera (PentaMax, Princeton Instruments, Inc). Image analysis and processing (flatfielding and background subtraction) were conducted using software supplied by Princeton Instruments (WinView/32) and Scion Corporation (Scion Image, version Beta 3b).

Patterned substrates, consisting of an array of squares having lateral dimensions of 5 x 5 $\mu m^2$ and ~185 nm deep, were fabricated following a previously published method (7) by microtransfer molding of thermal-set, optically-transparent epoxy on precleaned glass microscope slides. Al films were deposited on patterned substrates by thermal evaporation of Al at a rate of ~0.5 nm/s and base presssure of ca. 1.0 x $10^{-4}$ torr. The resulting metal thickness was ~200 nm, as measured by AFM. Corrosion studies were conducted at room temperature (25 $\pm$ 2 °C) under open circuit conditions by immersing the Al films into electrolyte solutions containing either 40 g/L sea salt (ASTM D-1141-52 simulated seawater solution, Lake Products) or 10 mM $H_2O_2$ (Fisher) in deionized water, with 7-hydroxycoumarin (~0.5 mM, Aldrich) added as a fluorescent imaging agent.

Recently, we have described novel imaging strategies that utilize solution fluorescence as a means for providing image contrast by a process of "backlighting" (8).

In this study, we also employ this approach. An illustrative representation of the experimental methodology is shown in Figure 2. By utilizing an intense light source in combination with a solution-phase fluorescent dye, high-resolution spatial surface maps of differential chemical reactivity can be obtained by optical microscopy configured in an epi-fluorescence setup. Thus, increases in spatially-localized fluorescence activity directly report on the localized corrosion process.

The films are patterned to monitor shape evolution during the initial stages of corrosion and to serve as a reference registry for pre- and post-surface characterization by ex-situ methods (e.g., AFM, XPS and EDX). A related methodology has been reported by Alkire et al. (9), but our technique differs slightly in that the lithographic pattern lies beneath the aluminum film. Since the aluminum films are deposited over the patterned grid, no additional contaminants are introduced from the patterning process.

## RESULTS AND DISCUSSION

In order to develop new methods and techniques for the study of corrosion processes, it is sometimes necessary to employ model systems. Recently, several researches have used thin films for this purpose (10). With thin-film reaction platforms, quantitative analysis of pitting corrosion is usually simplified since pits rapidly penetrate the film and reach an inert substrate. The pits then proceed to grow outward in a 2-D manner. Thin-film corrosion is also of appreciable intrinsic interest-for example, in the context of integrated electronic device stability. In any case, we also have applied a thin-film approach, in addition to employing microscopic patterned substrates. As will be demonstrated below, the combination of methodologies allows for monitoring of localized corrosion events at aluminum/aqueous interfaces to be temporally and spatially imaged and subsequently correlated with preexisting models.

### Structural Characterization of Patterned Thin-Films

The surface structure of thermally evaporated Al on patterned glass substrates is shown in Figure 3. Analysis of the images indicate that our film deposition conditions produce continuous, but fairly rough films (~50 nm (RMS) surface roughness) with a measured film thickness of c.a. 200 nm. Figure 3b shows a higher resolution AFM image of the local film microstructure, indicating the presence of rectangular-shaped grains ranging from ~0.06 to 0.24 $\mu m^2$ in size. This morphology is consistent with previous reports (11) for thermally evaporated Al films deposited at fairly low rates (~3 nm/s) and moderate base vacuum pressures (~$1.0 \times 10^{-4}$ torr).

### Monitoring of Gas Blistering and Film Delamination

Figure 4 shows results from experiments conducted on patterned Al thin-films exposed to an aerated aq. sea salt solution. We observe that the corrosion process is dominated by the evolution of gas which produces blisters and causes film delamination. The formation of a gas blister is shown in Figure 4a. Surprisingly, gas blister formation is sometimes observed in regions lacking appreciable localized pitting corrosion. Previous studies propose that the production of hydrogen and the formation of blisters is

a precursor to pitting (12). Figure 4 suggests that hydrogen evolution is involved in pit initiation rather than propagation.

The subsurface gas evolution process has the potential to exert large forces on the overlaying Al thin film. For instance, the pressure generated can be roughly estimated by

$$P = 1000\Gamma RT/d \qquad [1]$$

In eq [1], P is pressure, $\Gamma$ is film surface coverage, d is the film thickness, R is the gas constant and T is temperature. Using $\Gamma = 3.3 \times 10^{-9}$ mol/cm$^2$, R = 0.0821 L atm K$^{-1}$ mol$^{-1}$, d = $4.0 \times 10^{-8}$ cm and T = 298 K, for the oxidation of two monolayers of the metal film, the pressure generated is 2015 atm. While pressures this great are perhaps improbable, in real systems the calculation emphasizes that gas evolution can readily generate forces large enough to induce film blistering and delamination.

An example of rapid blister formation and growth is shown in Figure 4b. Time lapse images were taken over the period of ten minutes and difference-subtracted to emphasize the progression of blister growth. In Fig. 4b, the edge of a large blister (~0.5 mm dia.) grows from right to left. The dark areas in Fig. 4b correspond to the amount the blister grew over a specific time, as indicated above each image. From analysis of the optical images, the rate of blister growth is estimated to be ~2 $\mu m^2/s$. The presence of three pits, indicated by arrows, is also observable in Fig 4b. In contrast to the rapid growth of the blister, the areas of the pits grow at a much slower rate. However, as demonstrated above, very little aluminum needs to be oxidized in order to generate large amounts of gas. The presence of the small pits suggests these pits provide localized sites for gas generation. A number of researchers have indicated that the pH within a corrosion pit can be substantially lower than that of the bulk solution (13). The pH of a 40-g/l sea salt solution used in this experiment is 6.5. Assuming that the pH within the pits is significantly more acidic, a candidate reaction for the open-circuit generation of hydrogen gas is:

$$Al + 3H^+ + 2Cl^- \rightleftharpoons 3/2H_2 + AlCl_2^+ \qquad [2]$$

Since the hydrogen gas generated at the active sites (pits) can be dissipated easily, blister formation and growth need not be confined to regions where pits are observed. Presumably, significant film delamination occurs as a result of significant hydrogen evolution at small pits that nucleate at defect sites and grain boundaries.

An ex-situ AFM image of a highly-stressed Al thin-film after ~40 min exposure is shown in Fig. 4c. Large buckled regions can be observed which start and stop at the patterned edges of the thin film. These regions are the weakest stress points of the film and provide rupture points from which the subsurface gas can escape. Similar microscopic corrosion structures have been observed by Shimizu et al. (14) in AFM studies conducted on microtomed Al films, where significant surface restructuring can occur during the corrosion process.

Monitoring Pitting Corrosion

Figure 5 shows results from an experiment entailing exposure of a patterned Al thin-film to an aerated aq. 10 mM $H_2O_2$ solution. Pits are observed to nucleate and grow in a 2-D fashion via comparatively rapid dissolution of Al. However, not all pits initiate at the same time; for certain pits the initiation time is much longer, reflecting differences in localized activity. After a period of 21 min the Al films were significantly corroded. The onset and growth of single micron-sized pits are shown in Fig. 5b. The pit morphology was found to evolve with time. Initially, and at early times, the pit growth was uniform, extending radially-outward. However, at longer times the growing pit becomes more misshapen.

A plot of the pit perimeter and pit area versus time are shown in Fig. 5c. The pit perimeter varied linearly with time, while the pit area varied linearly with the square of time (see inset Fig 5c). An inflection point in both growth plots, however, is present at ~ 480 s. It is precisely at this point that pit growth becomes irregular. These observations are consistent with previous reports describing pitting corrosion of Al thin films in sodium chloride solutions (10a,15,16) which suggest that initially the pits grow uniformly because they are under diffusion control, while at longer times pit growth is irregular due to ohmic limitations. Note that the ohmic problem may be particularly complex here, since the only source of electrolyte for a local corrosion cell (apart from solvent autoprotolysis) is the corrosion reaction itself.

Based on a model put forth by Frankel (10a), the current density of a single pit can be estimated by

$$i = \frac{\rho n F 2 C_a}{M C_p} \qquad [3]$$

where $\rho$ is the density, $n$ is the number of electrons generated in the dissolution process ($3e^-$), $F$ is Faraday's constant, $M$ is the atomic weight, $C_a$ and $C_p$ are the slopes of the pit area versus time-squared and pit perimeter versus time plots, respectively. Substitution of the appropriate parameters yields a single pit current density of 5 $mA/cm^2$. This value is in good agreement with previous reports and falls within the range of values (4 to 47 $mA/cm^2$) determined by Hunkeler and Bohni (16) for aluminum foils exposed to various tap waters under open circuit conditions.

## SUMMARY

Newly developed methodologies to monitor localized corrosion of aluminum thin-films are presented. Preliminary experiments on two "model" corrosion systems (Al/sea salt and Al/$H_2O_2$) show differing types of corrosion behavior. For Al thin-films immersed in aq. sea salt solutions the corrosion process is dominated by excessive hydrogen gas evolution which results in significant film delamination. Pitting corrosion is observed but occurs on much slower time scales. In contrast, for Al thin-films exposed

to aq. hydrogen peroxide solutions pitting corrosion is governing mode of corrosion. Pit growth kinetics of single micron-sized etch pits were followed and found to be consistent with previously published models describing 2-D pit growth. Image analysis allowed for the estimation of single pit current densities under open circuit conditions.

## ACKNOWLEDGMENT

We gratefully acknowledge Prof. Richard Van Duyne and Ms. Michelle Duval for assistance with vapor deposition of Al thin films and the Office of Naval Research for financial support.

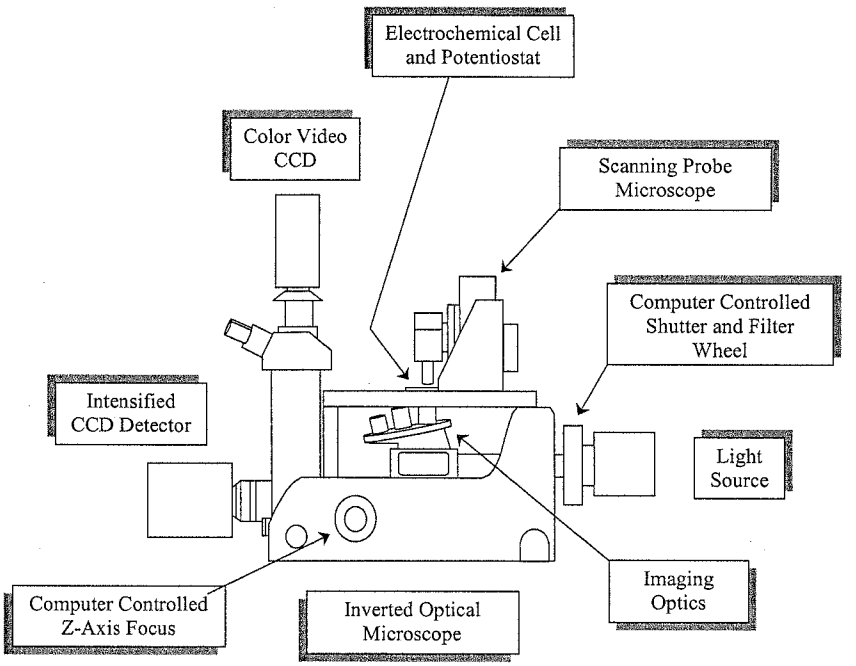


Figure 1. Schematic diagram of integrated optical and atomic force microscopies.

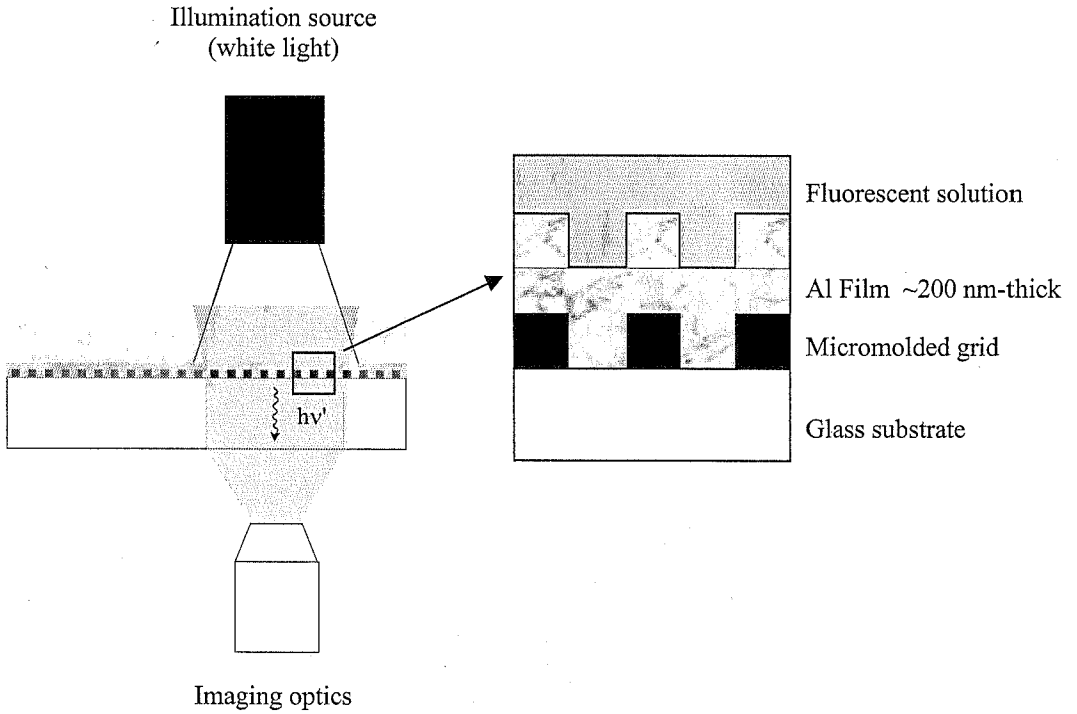


Figure 2. Illustrative representation of a "backlighting" optical microscopy experiment for measuring localized corrosion of a patterned Al thin-film. When the film corrodes the localized corrosion activity is imaged by the increase in fluorescence intensity, thus providing "reactive" image contrast. Figure is not drawn to scale.

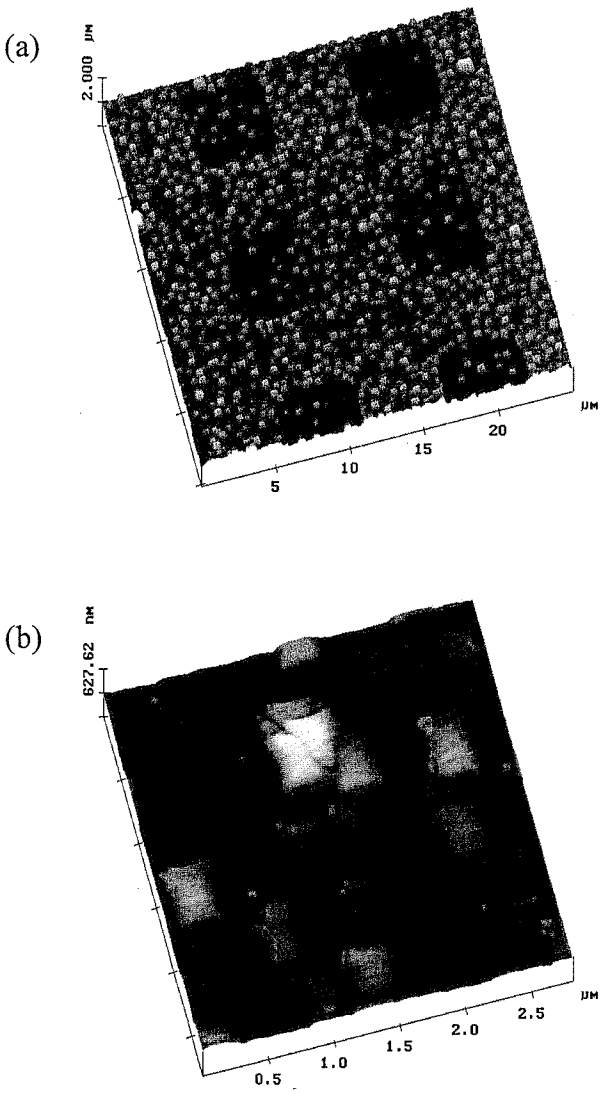


Figure 3. AFM images of patterned Al thin-films. (a) 25 x 25 $\mu m^2$ image (b) Higher resolution 2.7 x 2.7 $\mu m^2$ image showing local film microstructure.

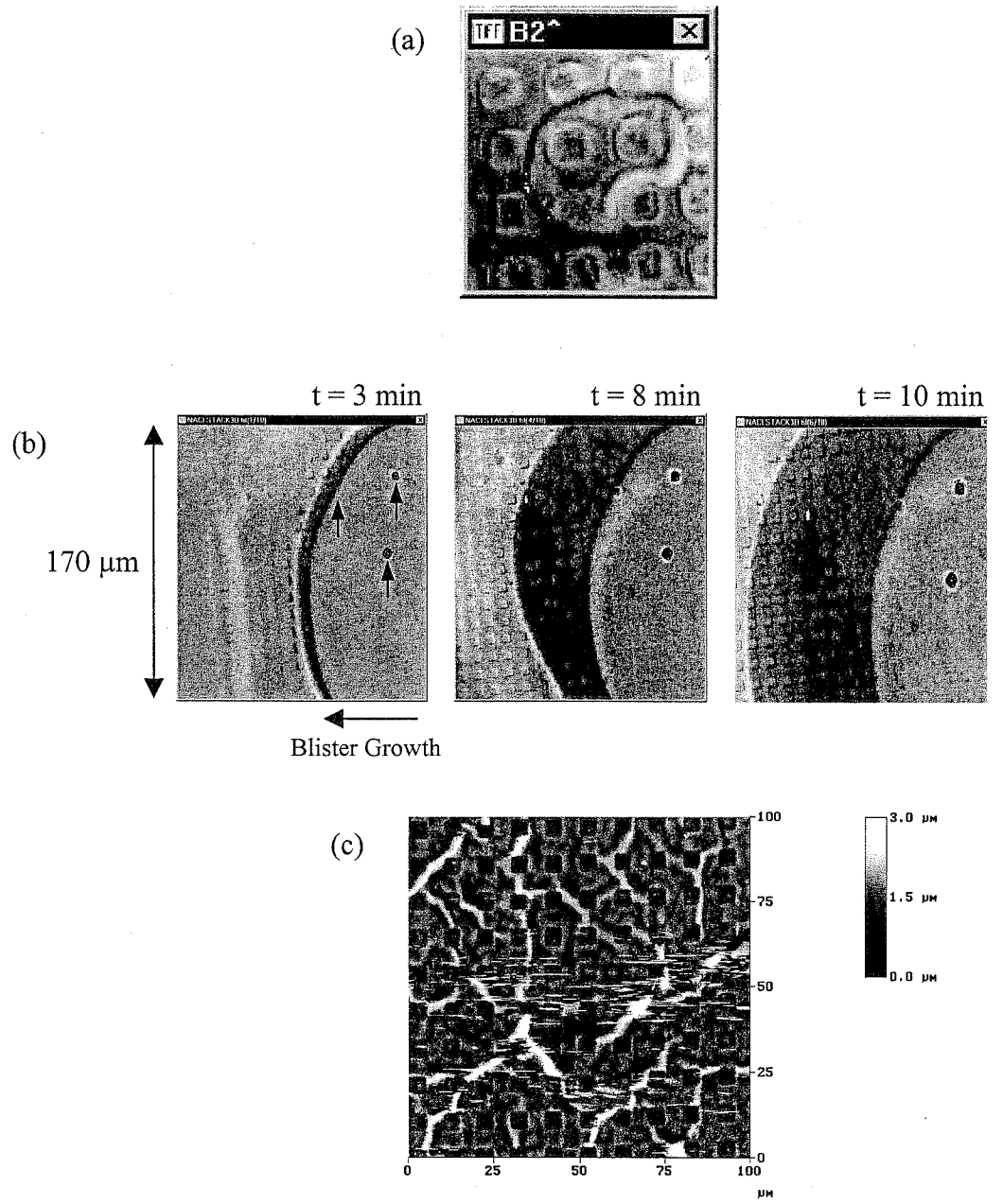


Figure 4. (a) Real-time optical (fluorescence) image of the initial stage of surface blistering of a microscopically-patterned Al thin-film due to hydrogen gas evolution in an aerated aq. 40 g/l sea salt solution. (b) Difference-subtraction time-lapse assessment of film delamination. Dark shaded areas indicate the amount of film delaminated over a set time. Times indicated above individual frames. Note the presence of three pits identified by the black arrows. (c) Ex-situ 100 x 100 $\mu m^2$ AFM image of a highly-stressed Al thin-film due to generation of hydrogen gas.

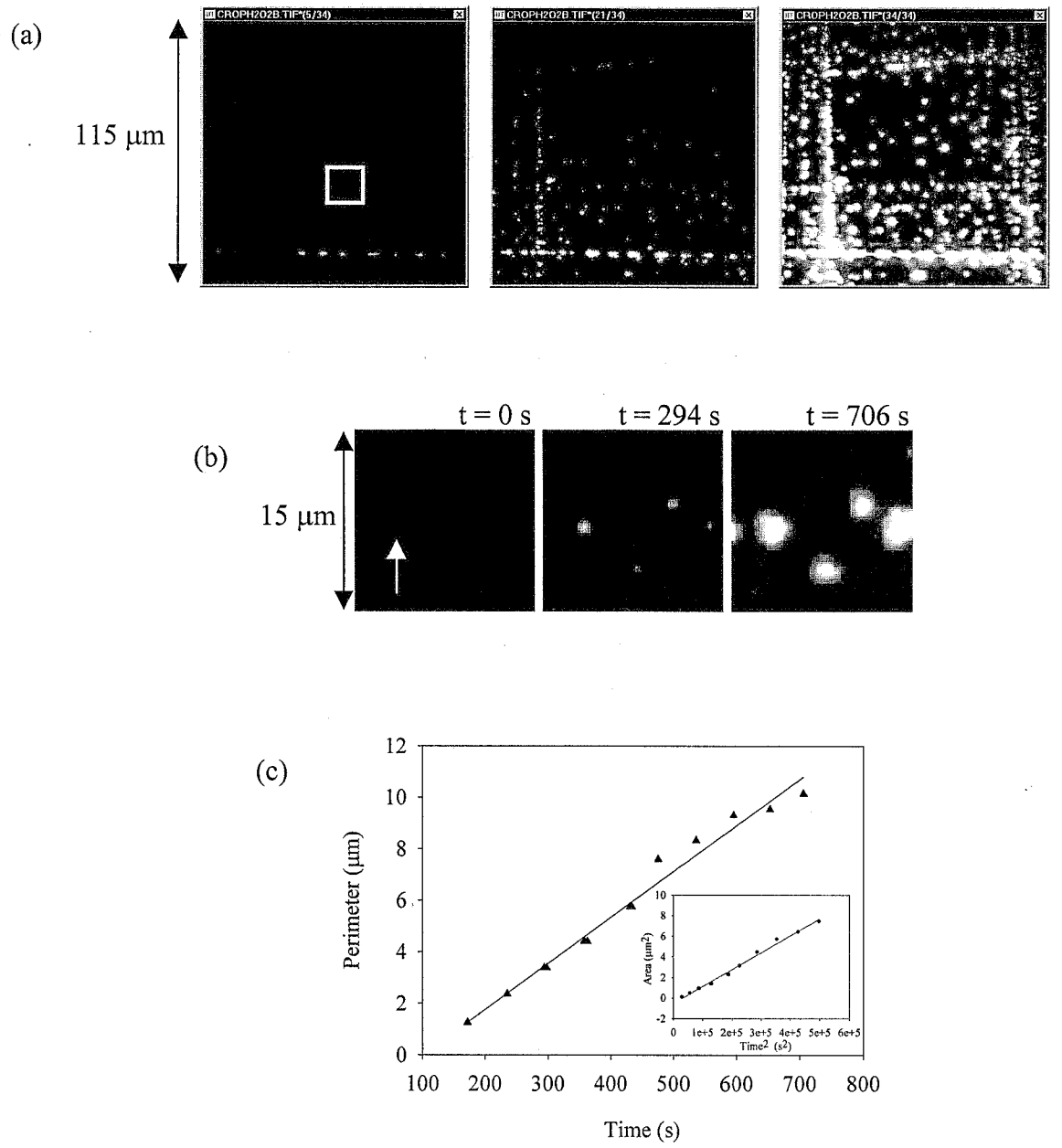


Figure 5. (a) Time lapse epi-fluorescence evaluation of incipient pitting corrosion of a patterned Al thin-film immersed in an aerated aq. 10 mM $H_2O_2$ solution. (b) High-resolution time lapse images showing onset and growth of pitting corrosion of the area indicated by the white box in (a). (c) Plot of pit perimeter versus time for the pit indicated by the white arrow in (b). Inset: plot of pit area versus time squared.

## REFERENCES


1. M. Alodan and W. H. Smyrl *J. Electrochem. Soc.* **145**, 1571 (1998).

2. G. Shi, L. F. Garfias-Mesias and W. H. Smyrl *J. Electrochem. Soc.* **145**, 2011 (1998).

3. (a) J. P. H. Sukamato, W. H. Smyrl, N. Casillas, M. Al-Odan, P. James, W. Jin, and L. Douglas. *Mater. Sci. Eng. A* 198, 17 (1995). (b) P. I. James, L. F. Garfias-Mesias, P. J. Moyer and W. H. Smyrl *J. Electrochem. Soc.* **145**, L64 (1998).

4. (a) R. C. Engstrom, C. M. Pharr, and M. D. Koppang *J. Electroanal. Chem.* **221**, 251 (1987). (b) R. C. Engstrom, K. W. Johnson and S. DesJarlais *Anal. Chem.* **59**, 670 (1987).

5. (a) S. Fiedler, R. Hagedorn, T. Schnelle, D. Richter, B. Wagner and G. Fuhr *Anal. Chem.* **67**, 820 (1995). (b) W. J. Bowyer, J. Xie and R. C. Engstrom *Anal. Chem.* **68**, 2005 (1996). (c) J. E. Vitt and R. C. Engstrom, Anal. Chem. **69**, 1070 (1997). (d) A. Panova, P. Pantano, and D. Walt *Anal. Chem.* **69**, 1635 (1997).

6. E.G. Dow, R. R. Bessette, G. L. Seeback, C. Marsh-Orndorff, H. Meunier, J. VanZee, and M. G. Medeiros *J. of Power Sources* **65**, 207 (1997).

7. K. J. Stevenson, G. J. Hurtt, and J. T. Hupp *Electrochemical and Solid-State Letters* **2**, 175 (1999).

8. K. J. Stevenson and J. T. Hupp in *New Directions in Electroanalytical Chemistry II*, J. Leddy, P. Vanysek, and M. D. Porter, Eds., Electrochemical Society: Princeton, NJ, Proceeding Vol. **99-5**, p. 37 (1999).

9. R. M. Rynders, C-H. Paik, R. Ke and R. C. Alkire *J. Electrochem. Soc.* **141**, 1439 (1994).

10. (a) G. S. Frankel *Corros. Sci.* **30**, 1203 (1990). (b) G. S. Frankel, J. O. Dukovic, V. Brusic, B. M. Rush, and C. V. James *J. Electrochem. Soc.* **139**, 2196 (1992). (c) G. S. Frankel, R. C. Newman, C. V. James and M. A. Russak *J. Electrochem. Soc.* **140**, 2192 (1993). (d) G. S. Frankel, J. R. Scully, and C. V. James *J. Electrochem. Soc.* **143**, 1834 (1996). (e) L. Balazs, J-F. Gouyet *Physica A* **217**, 319 (1995). (f) L. Balazs *Phys Rev. E* **54**, 1183 (1996) (e) Y-P. Zhao, C-F. Cheng, G-C. Wang, and T-M. Lu *Appl. Phys. Lett.* **73**, 2432 (1998).

11. C. W. Hollars and R. C. Dunn *Rev. of Sci. Inst.* **69**, 1747 (1998).

12. (a) C. B. Bargeron, R. B. Givens *Corrosion* **36**, 618 (1980).

13. (a) S. B. de Wexler and J. R. Galvele *J. Electrochem. Soc.* **121**, 1271 (1974). (b) K. Niscancioglu, K. Y. Davanger, and O. Strandmyr *J. Electrochem. Soc.* **128**, 1523 (1981).

14. K. Shimizu, K. Kobayashi, P. Skeldon, G. E. Thompson and G. C. Wood *Corros. Sci.* **39**, 701 (1997).

15. (a) K. P. Wong and R. C. Alkire *J. Electrochem. Soc.* **137**, 3010 (1990). (b) F. Hunkeler and H. Bohni *Corrosion* **37**, 645 (1981).

16. F. Hunkeler and H. Bohni *Corrosion* **40**, 534 (1984).